Journal of Materials Chemistry A

PAPER

View Article Online
View Journal

# Lithium–tellurium batteries based on tellurium/porous carbon composite

Cite this: DOI: 10.1039/c4ta02075h

Ying Liu,[a] Jiangwei Wang,[c] Yunhua Xu,[a] Yujie Zhu,[a] David Bigio[b] and Chunsheng Wang*[a]

Received 25th April 2014
Accepted 2nd June 2014

DOI: 10.1039/c4ta02075h

www.rsc.org/MaterialsA

For the first time, lithiation/delithiation behavior of tellurium at room temperature was investigated using tellurium/porous carbon (Te/C) composite electrodes. The Te/C composite is synthesized by the infusion of liquid tellurium into a porous carbon host at the high temperature of 600 °C under vacuum. Owing to the physical confinement of Te by porous carbon matrix, the Te/C electrode is capable of delivering a reversible volumetric capacity as high as 1400 mAh $cm^{-3}$ (224 mAh $g^{-1}$) at 312 mA $cm^{-3}$ (50 mA $g^{-1}$) current and maintains 87% of its initial capacity after 1000 cycles. Even when the current increases to 12480 mA $cm^{-3}$ (2000 mA $g^{-1}$), the Te/C electrode can still provide a volumetric capacity of 500 mAh $cm^{-3}$. The high volumetric capacity, long cycle life and good rate capability make Te/C composite a promising electrode for Li-ion batteries.

## Introduction

During the last two decades, rechargeable lithium-ion batteries (LIBs) have been widely used as the power sources for various mobile electronics, including cellular phones, laptop computers and digital cameras.[1–3] In recent years, the rapid development of electric vehicles (EVs), hybrid electric vehicles (HEVs) and large-scale renewable energy storage calls for batteries with high energy/power density, superior cycling and reliability stability, as well as low costs.[4–6] Recently, significant progress has been realized in the development of high capacity electrodes for LIBs. Due to the high capacity, materials based on elements in period 5 (In, Sn, Sb) and group 16 (chalcogen group: S and Se)[7–13] in the periodic table have been widely investigated as anodes and cathodes for Li-ion batteries, respectively. However, the lithiation/delithiation behavior of tellurium (Te), which is an element crossing period 5 and group 16, has not been studied yet. Owing to a large volume change of these high capacity electrodes, these materials will be cracked or even pulverized into powders after lithiation/delithiation, thus resulting in capacity decline. The most effective method is to disperse these materials into a porous carbon matrix to mechanically confine these cracked materials, thus improving the cycling stability.

In the chalcogen group, sulfur has been extensively studied as a cathode material for Li–S batteries because of its low cost and high theoretical gravimetric energy density (2570 Wh $kg^{-1}$).[14] However, sulfur cathodes are challenged by three major issues:[15–17] first, the electronic conductivity of S and formed $Li_2S$ are very low, resulting in a poor rate capability and low utilization of active materials. Second, the large volume expansion after lithiation (~80%) brings about particle pulverization and structure reorganization. Third, the dissolution of high order polysulfide intermediates into electrolyte and subsequent migration and reaction with Li anode lead to the transport of low-order polysulfides back to the cathode side, resulting in a "shuttle effect". Therefore, current Li–S batteries suffer from low coulombic efficiency and rapid capacity decay, blocking the commercialization of S cathode in the battery industry. Over the years, great efforts have been devoted to address these problems and many strategies have been proposed, such as impregnating sulfur into porous carbon,[18,19] encapsulating sulfur with graphene oxide[17] or conductive polymers,[20,21] entrapping sulfur into the yolk–shell structure,[16] or reducing the solubility of polysulfides by alternative electrolyte or additives.[22]

Recently, it has been reported that selenium (Se), which is an element in the chalcogen family (sulfur, selenium, tellurium), can also be treated as a perspective candidate for cathode material.[23–25] With similar chemical properties but higher electronic conductivity (Se: $1 \times 10^{-4}$ S $m^{-1}$, S: $5 \times 10^{-16}$ S $m^{-1}$), lithium–selenium (Li–Se) batteries can theoretically deliver a reversible gravimetric capacity of 675 mAh $g^{-1}$. However, although Se exhibits promising advantages compared with S, the electronic conductivity is still not high enough. Thus, inspired by this, tellurium, another element in the chalcogen family, which possesses the highest electronic conductivity among all non-metallic materials ($2 \times 10^{2}$ S $m^{-1}$), has additional advantages compared with sulfur and selenium such as

[a]Department of Chemical and Biomolecular Engineering, University of Maryland, College Park, Maryland 20742, USA. E-mail: cswang@umd.edu

[b]Department of Mechanical Engineering, University of Maryland, College Park, Maryland 20742, USA

[c]Department of Mechanical Engineering and Materials Science, University of Pittsburgh, Pittsburgh, Pennsylvania 15261, USA

high utilization rate and better kinetics during charge/discharge process. Despite the lower gravimetric capacity of tellurium electrode ($Li_2Te$: 419 mAh $g^{-1}$) than selenium ($Li_2Se$: 675 mAh $g^{-1}$) and sulfur ($Li_2S$: 1672 mAh $g^{-1}$), the higher density provides it a high volumetric capacity (2621 mAh $cm^{-3}$ based on a density of 6.24 g $cm^{-3}$), which is comparable to that of selenium (3253 mAh $cm^{-3}$ based on a density of 4.82 g $cm^{-3}$) and sulfur (3467 mAh $cm^{-3}$ based on a density of 2.07 g $cm^{-3}$). In fact, the battery packing space is usually limited in portable devices and EV/HEV; thus, volumetric capacity is actually more important than gravimetric capacity.[24,26] Therefore, the superior electronic conductivity, as well as high volumetric capacity, makes tellurium a potential candidate as electrode material in lithium-ion batteries.

In this study, a novel Te/C composite was synthesized by encapsulating liquid tellurium into the host of porous carbon at the high temperature of 600 °C under vacuum. For the first time, the lithiation/delithiation behavior of Te/C composite was investigated in 1 M $LiPF_6$ in a mixture of ethylene carbonate–diethyl carbonate (EC–DEC, 1 : 1 by volume) electrolyte at room temperature. The as-prepared Te/C electrode can deliver and maintain a reversible volumetric capacity of 1400 mAh $cm^{-3}$ (224 mAh $g^{-1}$) at a current rate of 50 mA $g^{-1}$ with a coulombic efficiency up to 99% for 1000 cycles. As the current density increases from 50 mA $g^{-1}$ to 1000 mA $g^{-1}$, 47% of the capacity is retained and goes down to 35% after the current density increases up to 2000 mA $g^{-1}$. The high volumetric capacity, long cycle life, excellent coulombic efficiency and good rate capability of Li–Te battery demonstrate that tellurium is a perspective electrode material for high-energy storage and large-scale applications.

## Experimental section

### synthesis of tellurium/porous carbon composite

The Te/C composite was synthesized by impregnating liquid tellurium into porous carbon (Advanced Chemical Supply Inc., USA) matrix through a vacuum-liquid-infusion method. Typically, solid tellurium and porous carbon were mixed with a ratio of 1 : 1 by weight and sealed in a glass tube under vacuum. Heat treatment at 600 °C was conducted to melt the solid tellurium (melting point is 450 °C) and infuse it into the porous carbon.

### Material characterization

Scanning electron microscopy (SEM) images were taken using a Hitachi SU-70 analytical ultra-high resolution SEM (Japan). Transmission electron microscopy (TEM) images were taken by JEOL (Japan) 2100F field-emission TEM. Thermogravimetric analysis (TGA) was carried out using a thermogravimetric analyzer (TA instruments, USA) with a heating rate of 10 °C $min^{-1}$ in air. X-ray diffraction (XRD) pattern was recorded by Bruker Smart1000 (Bruker AXS Inc., USA) using CuK$\alpha$ radiation. Brunauer–Emmett–Teller (BET) specific surface area and pore size/volume were tested using $N_2$ absorption on Micromeritics ASAP 2020 (Micromeritics Instrument Corp., USA). Raman measurements were performed on a Horiba Jobin Yvon Labram Aramis using a 532 nm diode-pumped solid-state laser, attenuated to give ~900 μW power at the sample surface.

### Electrochemical measurements

Te/C composite was mixed with carbon black and sodium alginate binder to form a slurry at the weight ratio of 70 : 15 : 15. The electrode was prepared by casting the slurry onto aluminum (Al) foil using a doctor blade and drying at room temperature overnight, followed by heating at 100 °C in a vacuum oven overnight. The same method was used to fabricate the pure tellurium and porous carbon electrodes. The thickness of the coating on Al is approximately 20 μm and the loading of electrode is about 1 mg $cm^{-2}$. The electrode was cut into circular pieces with a diameter of 1.2 cm for coin-cell testing. Li-ion batteries were assembled with lithium as the counter electrode, 1 M $LiPF_6$ in a mixture of ethylene carbonate–diethyl carbonate (EC–DEC, 1 : 1 by volume) as the electrolyte, and Celgard®3501 (Celgard, LLC Corp., USA) as the separator. Electrochemical performance was tested using an Arbin battery test station (BT2000, Arbin Instruments, USA). Capacity was calculated on the basis of the mass of Te. GITT measurements were carried out by applying a pulse constant current (50 mA $g^{-1}$) with duration of 0.25 h, followed by a 6 h relaxation to reach an equilibrium potential. Cyclic voltammograms at a scan rate of 0.1 mV $s^{-1}$ between 0.8 and 2.5 V (*vs.* $Li/Li^+$) were obtained using Solartron 1260/1287 electrochemical interface (Solartron Metrology, UK).

## Results and discussion

Fig. 1a and b show the SEM and TEM images of Te/C composite, which exhibits a well-formed flake-like shape. As compared with the pure porous carbon, illustrated in the inset of Fig. 1a, no morphology change can be observed after tellurium is infused into the porous carbon host. This indicates that most of the tellurium has filled the inside of the porous carbon, which can be confirmed by the high resolution TEM images of Te/C composite (Fig. 1c). The elemental mapping images (Fig. 1d, e and f) reveal that tellurium is homogeneously distributed in the porous carbon matrix and no tellurium accumulation is observed on the carbon surface, illustrating a perfect Te infiltration into the porous carbon. The uniform distribution of tellurium free of surface accumulation, as well as excellent electronic conductivity of both carbon and tellurium, ensure a high utilization of active materials and good kinetics during electrochemical reactions.

The content of tellurium in Te/C composite is revealed to be at 50 wt% by the TEM elemental analysis (Fig. 1g), which is further confirmed by the TGA measurement results as shown in Fig. 1h. There is no weight loss observed from room temperature to 350 °C, indicating that the composite is stable up to 350 °C in air and that no Te oxidation and carbon decomposition reaction occur in the range of 25–350 °C. The weight loss from 350 to 480 °C is a combination of weight loss from the carbon oxidation to carbon dioxide, $C + O_2 = CO_2$, and weight increase due to the oxidation of tellurium, $Te + O_2 = TeO_2$. The

 

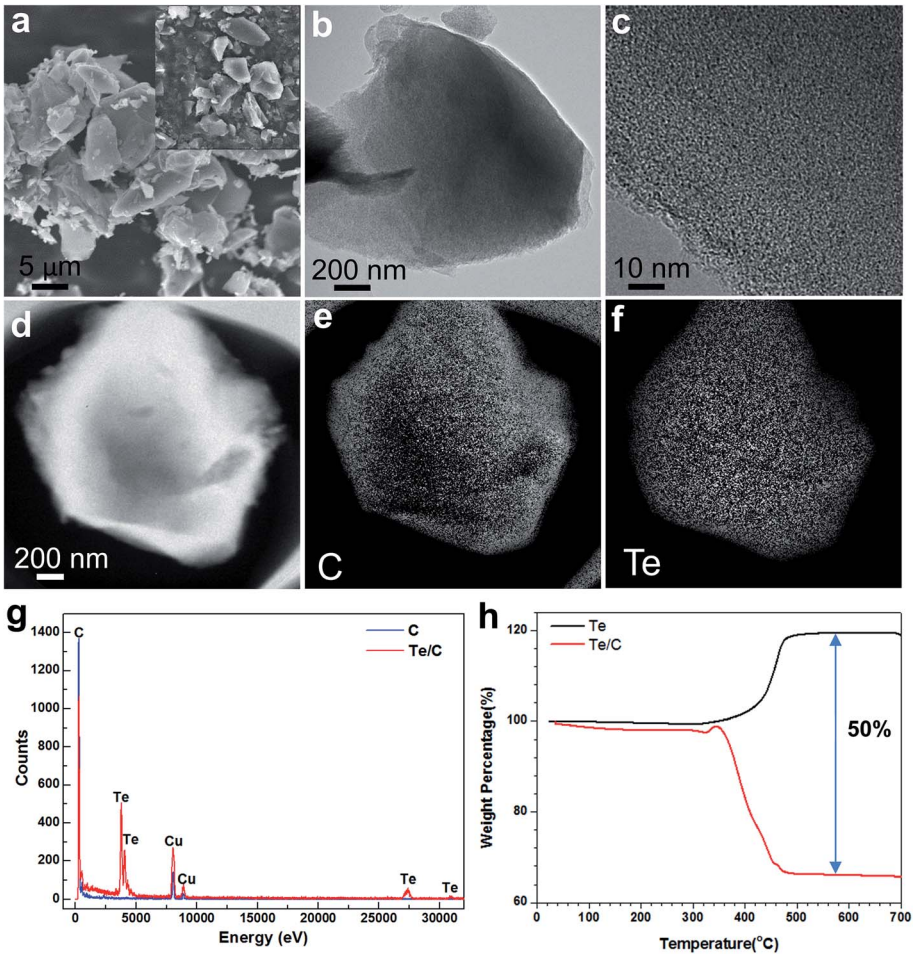


Fig. 1 (a) SEM images of the tellurium-impregnated porous carbon composite, inset image is the pure porous carbon. (b) and (c) TEM images of Te/C composite. TEM and elemental mapping images of (d) Te/C composite, (e) carbon and (f) tellurium. (g) TEM elemental analysis. (h) TGA results of Te/C composite and pristine Te.

Te content was determined to be 50% using the following equation:

$$\text{Te (wt\%)} = \frac{\text{molecular weight of Te}}{\text{molecular weight of } TeO_2} \times \frac{\text{final weight of } TeO_2}{\text{initial weight of Te/C}} \times 100$$

The tellurium impregnation into porous carbon is also evidenced by the Brunauer–Emmett–Teller (BET) analysis, as shown in Fig. 2a. The specific surface area is calculated from the adsorption data in the relative pressure range of 0.05 to 0.3. Total pore volumes were calculated from the amount of adsorption at a relative pressure, $P/P_0$, of 0.90. Micropore volumes were calculated using the *t*-plot method. The porous carbon has a large BET surface area of 1416 $m^2\ g^{-1}$ and a high pore volume of 0.44 $cm^3\ g^{-1}$. After infusion of tellurium, the BET surface area decreased dramatically to 353 $m^2\ g^{-1}$, and the pore volume declined to 0.06 $cm^3\ g^{-1}$, indicating that most of the pores have been occupied by Te. This result could also be confirmed by the pore-size distribution curves (Fig. 2b), which were determined from the adsorption branches of the isotherms using density functional theory (DFT), *i.e.*, apparent decrease of the pore size was observed after porous carbon was infused by Te.

The infused tellurium in porous carbon exists in crystal structure as demonstrated by the XRD patterns of Te/C composite in Fig. 2c. For comparison, the XRD patterns of both pristine Te and pure porous carbon are also shown in Fig. 2c. The Te/C composite displays well-defined diffraction pattern as the pristine tellurium (JCPDA File no. 79-0736). The nature of tellurium in composite is further characterized using Raman spectroscopy. For comparison, porous carbon (C), pristine Te (Te), and manually mixed Te–C composite (Te&C) at the same ratio to the Te/C composite in room temperature, were also analyzed using Raman spectroscopy (Fig. 2d). For porous carbon, two broad peaks at 1350 $cm^{-1}$ and 1590 $cm^{-1}$ are attributed to the disordered (D) and graphitic (G) carbon, demonstrating that the porous carbon is partially graphitized. Typical Raman spectrum pattern of pristine tellurium is characterized by three peaks from 80 to 700 $cm^{-1}$, which are probably attributed to the $E_2$ bond–bending, $A_1$ bonding-bending

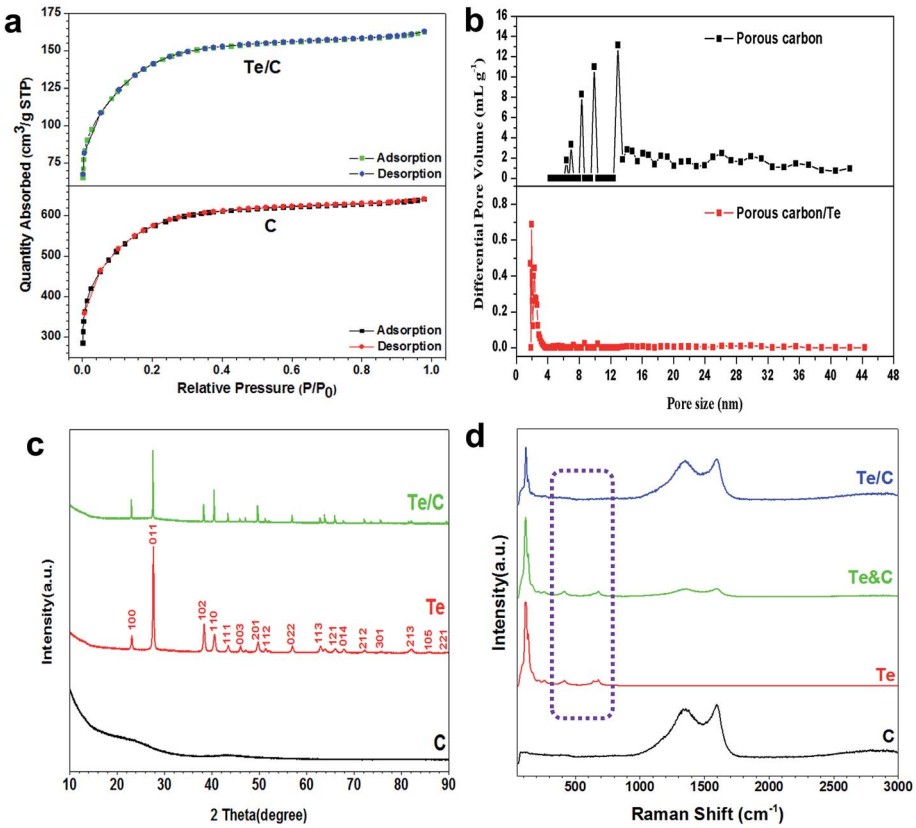


Fig. 2 (a) BET Adsorption and desorption curve of the porous carbon and Te/C composite. (b) DFT pore-size distribution of porous carbon and Te/C composite. (c) XRD pattern of porous carbon, pristine Te and Te/C composite. (d) Raman spectra of porous carbon, pristine Te, manually mixed Te&C, and Te/C composite.

and $A_1$ bond-stretching modes of the crystalline trigonal tellurium with a highly anisotropic crystal structure consisting of helical chains covalently bound to each other.[27,28] For Te/C composite, after infusing tellurium into the porous carbon host, two small peaks from 400 to 700 $cm^{-1}$ disappear, although the vibration peaks around 117 $cm^{-1}$ of Te remains, indicating that the Te is not only physically confined in porous carbon matrix, but is also chemically bonded to carbon, thus stabilizing tellurium in the supporting carbon matrix. The chemical bonding is probably induced by high temperature infusion process since the Te peak at 400 to 700 $cm^{-1}$ still exists in the Te&C mixture prepared at room temperature (Fig. 2d). The mixed Te&C exhibits the simple addition of tellurium and carbon Raman spectra separately without any changes on the forms of Te itself. Therefore, the confinement of the porous carbon at high temperature altered the structure of tellurium remarkably.

The electrochemical performance of the Te/C composite was investigated in coin cells using lithium metal as the counter electrode, and 1 M $LiPF_6$ in a mixture of ethylene carbonate–diethyl carbonate (EC–DEC, 1 : 1 by volume) as the electrolyte. All electrochemical experiments were conducted at room temperature, and all capacity was calculated based on the mass or volume of tellurium. For Te/C composite, the current density was calculated on the basis of the total weight of tellurium and porous carbon. Fig. 3 shows the charge/discharge profiles of Te/C composite between 0.8 and 2.5 V at a current density of 50 mA $g^{-1}$ with the comparison of both pristine Te and porous carbon electrodes under the same voltage range and current density. As demonstrated in Fig. 3a, pristine Te electrode shows a voltage plateau at 1.6 V in discharge and at 1.8 V in charge with a discharge volumetric capacity of 1685 mAh $cm^{-3}$ (270 mAh $g^{-1}$) and charge volumetric capacity of 936 mAh $cm^{-3}$ (150 mAh $g^{-1}$) in the first cycle. The plateau at 0.9 V is attributed to the decomposition of electrolyte and formation of solid electrolyte interphase (SEI). For Te/C composite (Fig. 3b), two slope-shaped voltage plateaus located at 1.6 V and 1.4 V in discharge, and 1.7 V and 1.9 V in charge process are observed. The extra voltage plateau at 1.4 V for discharge and 1.7 V for charge cannot be attributed to carbon since no voltage plateau above 1.0 V is observed in electrode made by pure porous carbon (Fig. 3c). The transition from well-defined single plateau of pure Te to two slope-shaped plateaus of Te/C is probably due to the interaction between Te and porous carbon, which is also observed in the S/C and Se/C composites.[17,19,20] The interaction between Te and porous carbon was confirmed by Raman measurement in Fig. 2c. The Te/C composite delivers a volumetric capacity of 6739 mAh $cm^{-3}$ (1080 m Ah $g^{-1}$) in the first discharge and 1872 mAh/$cm^3$ (300 mAh $g^{-1}$) in the first charge process. The large irreversible capacity formed in the first cycle is mainly attributed to the formation of SEI film on the porous carbon,[25] which is confirmed by the high irreversible capacity of porous carbon itself in Fig. 3c. Since the porous carbon only provides 6 mAh

 

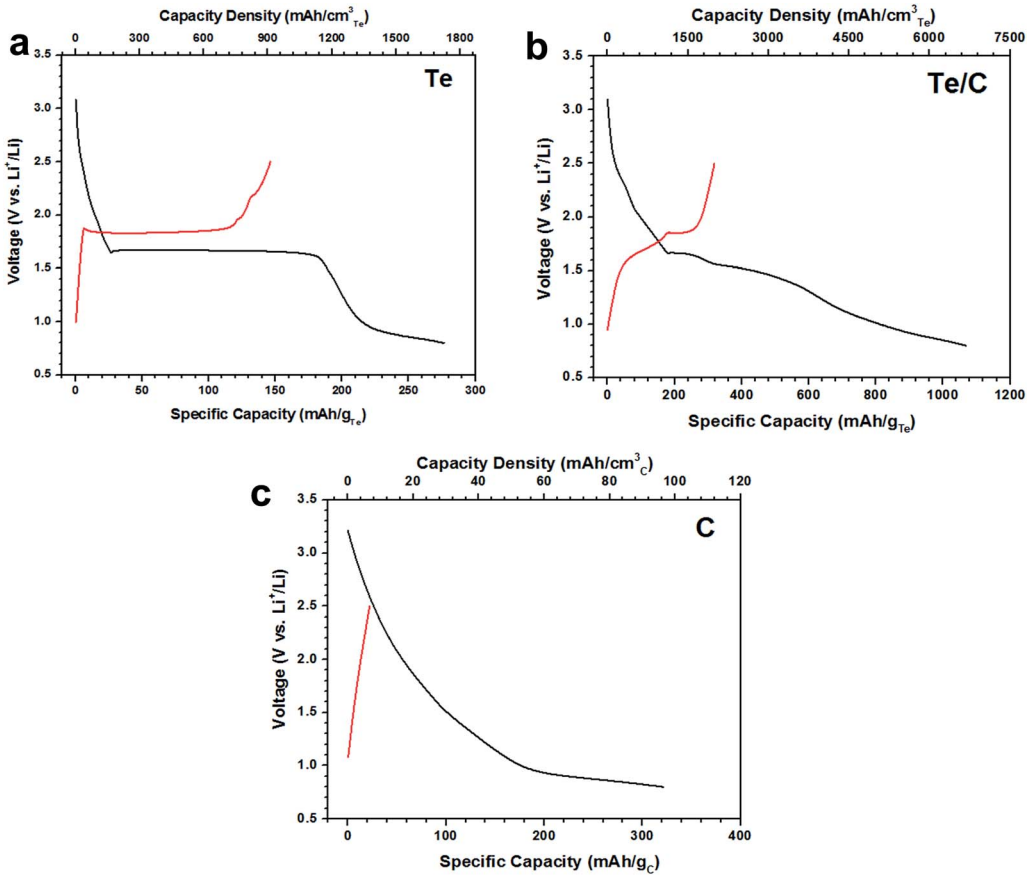


Fig. 3 Charge/discharge profiles at the first cycle of (a) pristine Te electrode, (b) Te/C composite electrode and (c) porous carbon electrode.

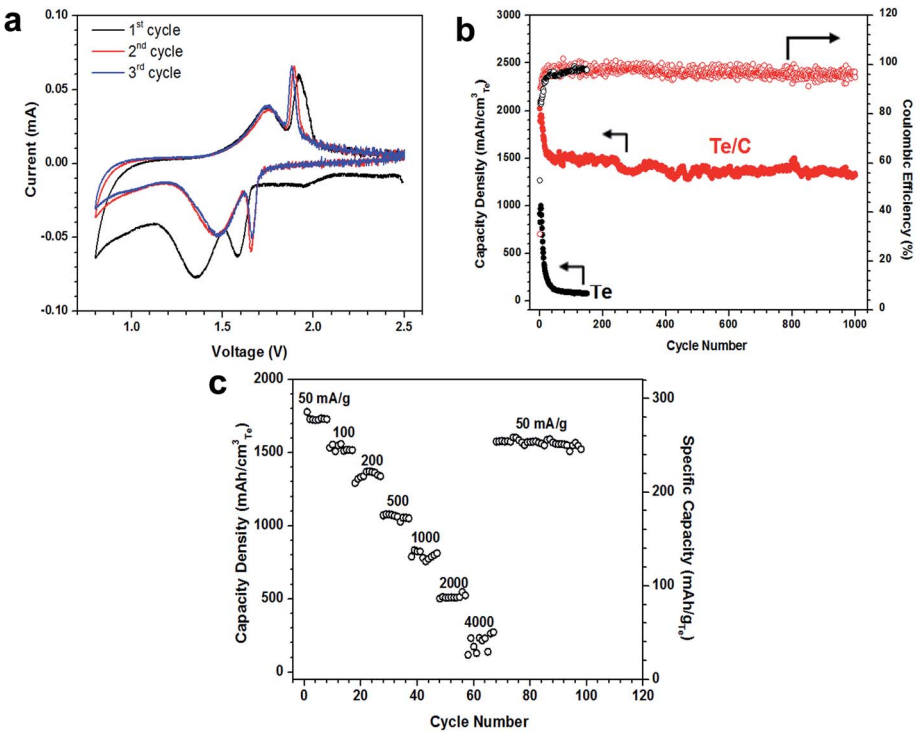


Fig. 4 (a) Cyclic voltammograms of the Te/C composite electrode in the initial three cycles. (b) Cycling performance and coulombic efficiency of the Te/C composite and pristine Te electrode. (c) Rate capability of the Te/C composite electrode in Li–Te batteries.

$cm^{-3}$ volumetric capacity (20 mAh $g^{-1}$) (Fig. 3c), the contribution from carbon to the total capacity of Te/C is negligible.

Aside from charge/discharge profiles, cyclic voltammetry (CV) can reveal more details about the electrochemical reaction during the lithiation/delithiation process. Fig. 4a demonstrates the CV of the Te/C composite at a scan rate of 0.1 mV $s^{-1}$ between 0.8 V and 2.5 V. Two redox couples are observed with the reduction/oxidation peaks located at 1.6/1.9 V and 1.4/1.7 V separately, which is in good agreement with the double slope plateaus of charge/discharge curves in Fig. 3b. After the first cycle, the two cathodic peaks shift to a higher voltage, while the anodic peaks shift slightly to a lower voltage, reducing the potential hysteresis for lithiation and delithiation. The reduction of overpotential after the first cycle has been observed in many high capacity electrodes, which is believed to be associated with the relaxation of stress/strain induced by volume expansion after first lithiation through deformation.[25] Moreover, the stable cathodic/anodic peaks after the first cycle indicate a high cycling stability.

The cycling performance of Te/C composite is investigated by galvanostatic charge and discharge of the Te/C composite electrodes between 0.8 V and 2.5 V at a current density of 50 mA $g^{-1}$ for 1000 cycles, as shown in Fig. 4b. The Te/C composite provides a volumetric capacity of 2022 mAh $cm^{-3}$, corresponding to a specific capacity of 324 mAh $g^{-1}$ in the first delithiation process, which is close to the theoretical capacity of Te. In addition, a reversible volumetric capacity of 1400 mAh $cm^{-3}$ (224 mAh $g^{-1}$) is still retained even after 1000 cycles, with columbic efficiency always approaching up to 99% except the first cycle, indicating an excellent cycling stability. For comparison, the cycling stability of pristine Te electrode was also tested under the same electrochemical condition, which suffered severely from rapid capacity fading and retained only 7% of the initial capacity after a mere 20 cycles. Therefore, after mechanical confinement and chemical stabilization of tellurium in the supporting carbon host, the Te/C composite produced possesses superior electrochemical performance with a high volumetric capacity and long cycle life.

In addition to the good cycling stability, the Te/C electrode also displays a high rate capability. As shown in Fig. 4c, when the current density increases from 50 to 1000 mA $g^{-1}$ and 2000 mA $g^{-1}$, the volumetric capacity of the Te/C composite retains about 47% and 35% of capacity at 50 mA $g^{-1}$, respectively. Even when the Te/C composite is charged/discharged at 4000 mA $g^{-1}$, 17% capacity retention can still be obtained. The superior volumetric capacity, high coulombic efficiency, long cycle life and good rate capability of Te/C composite demonstrate that tellurium is a promising electrode material candidate for Li-ion batteries, especially in large-scale energy storage applications.

To investigate the reaction kinetics of Te/C composite at different lithiation/delithiation states, the overpotential and reaction resistance of Te/C electrodes during charge/discharge were analyzed using the galvanostatic intermittent titration technique (GITT). During the GITT measurements, the Te/C electrodes were charged/discharged by a series of constant current pulse of 50 mA $g^{-1}$ with an equal duration period of 0.25 h. Following each pulse, the cells were left at open circuit state for 6 h to reach the equilibrium potentials. Fig. 5a demonstrates the potential response of Te/C electrode during GITT measurement in Li-ion batteries. The dotted-lines represent the equilibrium open circuit potentials (OCPs). The reaction resistance at different Li ion insertion and extraction levels was also calculated by dividing the overpotential by the pulse current (Fig. 5b). The overpotential and reaction resistance of the Te/C electrode generally increase with state of charge/discharge. For lithiation, the reaction resistance levels off after 50% of discharge, while the resistance rises expeditiously at the end of charge. The different behavior of reaction resistance between charge and discharge may be attributed to the electronic contact resistance that decreases with volume expansion during lithiation and increases with volume contraction during delithiation.

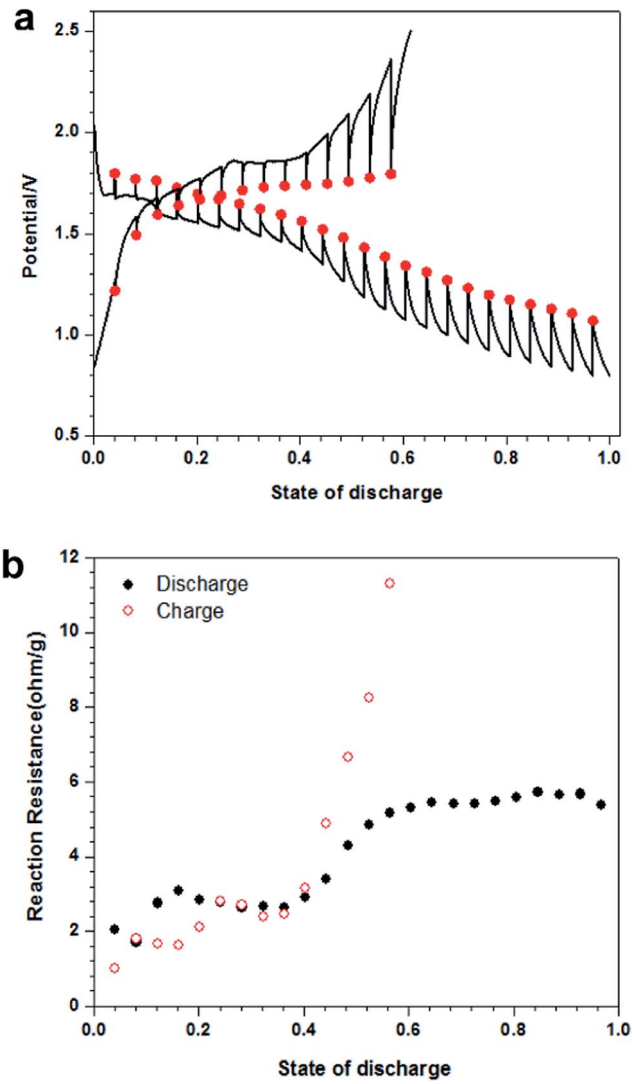


Fig. 5 (a) Potential response and (b) reaction resistance of the Te/C composite electrode during GITT measurement. Note: current density was calculated on the basis of the total weight of porous carbon and Te.

## Conclusion

In summary, a novel tellurium/porous carbon (Te/C) composite is synthesized at a high temperature of 600 °C under vacuum. The designed Te/C composite is employed, for the first time, as an electrode material in lithium-ion batteries, which exhibits excellent electrochemical performance in commercialized carbonate-based electrolyte. Owing to the physical confinement and chemical stabilization of tellurium in the supporting carbon matrix, the Te/C electrode can deliver a reversible volumetric capacity of 1400 mAh $cm^{-3}$ (224 mAh $g^{-1}$) and a high coulombic efficiency over 99% up to 1000 cycles without any further capacity decay. The high volumetric capacity, long cycle life, excellent coulombic efficiency and good rate capability of Te/C composite demonstrate that Li–Te batteries are promising candidates for applications in large-scale and high-energy storage.

## Acknowledgements

We acknowledge the technical support of the University of Maryland Nano Center and its NispLab.

## References

1 J. M. Tarascon and M. Armand, *Nature*, 2001, **414**, 359–4288.
2 K. S. Kang, Y. S. Meng, J. Breger, C. P. Grey and G. Ceder, *Science*, 2006, **311**, 977–4288.
3 Q. Q. Xiong, Y. Lu, X. L. Wang, C. D. Gu, Y. Q. Qiao and J. P. Tu, *J. Alloys Compd.*, 2012, **536**, 219–4288.
4 M. Armand and J. M. Tarascon, *Nature*, 2008, **451**, 652–4288.
5 J. W. Wang, X. H. Liu, K. Zhao, A. Palmer, E. Patten, D. Burton, S. X. Mao, Z. Suo and J. Y. Huang, *ACS Nano.*, 2012, **6**, 9158–4288.
6 J. B. Goodenough and Y. Kim, *Chem. Mater.*, 2010, **22**, 587–4288.
7 S. A. Webb, L. Baggetto, C. A. Bridges and G. M. Veith, *J. Power Sources*, 2014, **248**, 1105–4288.
8 Y. Xu, Y. Zhu, Y. Liu and C. Wang, *Adv. Energy Mater.*, 2013, **3**, 128–4288.
9 P. Meduri, C. Pendyala, V. Kumar, G. U. Sumanasekera and M. K. Sunkara, *Nano Lett.*, 2009, **9**, 612–4288.
10 T. Ramireddy, M. M. Rahman, T. Xing, Y. Chen and A. M. Glushenkov, *J. Mater. Chem. A.*, 2014, **2**, 4282–4288.
11 C. B. Bucur, J. Muldoon, A. Lita, J. B. Schlenoff, R. A. Ghostine, S. Dietz and G. Allred, *Energy Environ. Sci.*, 2013, **6**, 3286–4288.
12 H. Kim, J. T. Lee, D. C. Lee, A. Magasinski, W. Cho and G. Yushin, *Adv. Energy Mater.*, 2013, **3**, 1308–4288.
13 H. T. Kwon and C. M. Park, *J. Power Sources*, 2014, **251**, 319–4288.
14 P. G. Bruce, S. A. Freunberger, L. J. Hardwick and J.-M. Tarascon, *Nat. Mater.*, 2012, **11**, 19–4288.
15 J. Guo, Y. Xu and C. Wang, *Nano Lett.*, 2011, **11**.
16 Z. W. She, W. Li, J. J. Cha, G. Zheng, Y. Yang, M. T. McDowell, P.-C. Hsu and Y. Cui, *Nat. Commun.*, 2013, **4**, 1331–4288.
17 H. Wang, Y. Yang, Y. Liang, J. T. Robinson, Y. Li, A. Jackson, Y. Cui and H. Dai, *Nano Lett.*, 2011, **11**, 2644–4288.
18 X. Ji, K. T. Lee and L. F. Nazar, *Nat. Mater.*, 2009, **8**, 500–4288.
19 J. Schuster, G. He, B. Mandlmeier, T. Yim, K. T. Lee, T. Bein and L. F. Nazar, *Angew. Chem., Int. Ed.*, 2012, **51**, 3591–4288.
20 J. Wang, J. Yang, J. Xie and N. Xu, *Adv. Mater.*, 2002, **14**, 963–4288.
21 L. Xiao, Y. Cao, J. Xiao, B. Schwenzer, M. H. Engelhard, L. V. Saraf, Z. Nie, G. J. Exarhos and J. Liu, *Adv. Mater.*, 2012, **24**, 1176–4288.
22 E. S. Shin, K. Kim, S. H. Oh and W. I. Cho, *Chem. Commun.*, 2013, **49**, 2004–4288.
23 A. Abouimrane, D. Dambournet, K. W. Chapman, P. J. Chupas, W. Weng and K. Amine, *J. Am. Chem. Soc.*, 2012, **134**, 4505–4288.
24 C.-P. Yang, S. Xin, Y.-X. Yin, H. Ye, J. Zhang and Y.-G. Guo, *Angew. Chem., Int. Ed.*, 2013, **52**, 1–4288.
25 C. Luo, Y. Xu, Y. Zhu, Y. Liu, S. Zheng, Y. Liu, A. Langrock and C. Wang, *ACS Nano*, 2013, **7**, 8003–4288.
26 H. S. Kim, T. S. Arthur, G. D. Allred, J. Zajicek, J. G. Newman, A. E. Rodnyansky, A. G. Oliver, W. C. Boggess and J. Muldoon, *Nat. Commun.*, 2011, **2**, 427–4288.
27 V. V. Poborchii, *Solid State Commun.*, 1998, **107**, 513–4288.
28 J.-M. Song, Y.-Z. Lin, Y.-J. Zhan, Y.-C. Tian, G. Liu and S.-H. Yu, *Cryst. Growth Des.*, 2008, **8**, 1902–4288.